


Combining high spatial resolution multi-temporal satellite data with leaf-on LiDAR to enhance tree species discrimination at the crown level

Fang Fang, Brenden E. McNeil, Timothy A. Warner & Aaron E. Maxwell


To cite this article: Fang Fang, Brenden E. McNeil, Timothy A. Warner & Aaron E. Maxwell (2018) Combining high spatial resolution multi-temporal satellite data with leaf-on LiDAR to enhance tree species discrimination at the crown level, *International Journal of Remote Sensing*, 39:23, 9054-9072, DOI: [10.1080/01431161.2018.1504343](https://doi.org/10.1080/01431161.2018.1504343)

To link to this article: <https://doi.org/10.1080/01431161.2018.1504343>

 View supplementary material 

 Published online: 02 Aug 2018.

 Submit your article to this journal 

 Article views: 108

 View Crossmark data 



Combining high spatial resolution multi-temporal satellite data with leaf-on LiDAR to enhance tree species discrimination at the crown level

Fang Fang , Brenden E. McNeil, Timothy A. Warner and Aaron E. Maxwell

Department of Geology and Geography, West Virginia University, Morgantown, WV, USA

ABSTRACT

The long-standing goal of discriminating tree species at the crown-level from high spatial resolution imagery remains challenging. The aim of this study is to evaluate whether combining (a) high spatial resolution multi-temporal images from different phenological periods (spring, summer and autumn), and (b) leaf-on LiDAR height and intensity data can enhance the ability to discriminate the species of individual tree crowns of red oak (*Quercus rubra*), sugar maple (*Acer saccharum*), tulip poplar (*Liriodendron tulipifera*), and black cherry (*Prunus serotina*) in the Fernow Experimental Forest, West Virginia, USA. We used RandomForest models to measure a loss of classification accuracy caused by iteratively removing from the classification one or more groups from six groups of variables: spectral reflectance from all multi-spectral bands in the (1) spring, (2) summer, and (3) autumn images, (4) vegetation indices derived from the three multispectral datasets, (5) canopy height and intensity from the LiDAR imagery, and (6) texture related variables from the panchromatic and LiDAR datasets. We also used ANOVA and decision tree analyses to elucidate how the multispectral and LiDAR datasets combine to help discriminate tree species based on their unique phenological, spectral, textural, and crown architectural traits. From these results, we conclude that combining high spatial resolution multi-temporal satellite data with LiDAR datasets can enhance the ability to discriminate tree species at the crown level.

ARTICLE HISTORY

Received 2 February 2018

Accepted 29 June 2018

KEYWORDS

Phenology; LiDAR; classification; texture; multi-spectral; tree species; crown architecture

1. Introduction

Obtaining spatially explicit data on tree species composition can lead to improved management of biodiversity and the provision of ecosystem services related to air and water quality (Dwyer, Nowak, and Noble 2003; Karlson et al. 2016). Tree species information is traditionally derived via field survey or aerial interpretation (Pu and Landry 2012), which is time-consuming and quite limited for broad-scale tree species mapping. To date, with the growing availability of high-spatial resolution and high-spectral resolution images from various sensors, researchers are increasingly using imagery to classify

CONTACT Fang Fang fafang@mix.wvu.edu Department of Geology and Geography, West Virginia University, Morgantown, WV, USA

Supplemental data can be accessed [here](#).

© 2018 Informa UK Limited, trading as Taylor & Francis Group

individual trees in both rural and urban settings (Alonzo, Bookhagen, and Roberts 2014; Cho, Malahlela, and Ramoelo 2015; Cochrane 2000; Colgan et al. 2012; Dalponte et al. 2013; Immitzer, Atzberger, and Koukal 2012; Key et al. 2001; Melgani and Bruzzone 2004; Omer et al. 2016; Pu and Landry 2012; Van Ewijk et al. 2014; Verlič et al. 2014; Waser et al. 2014; Zhang and Hu 2012). These studies not only illustrate the potential to discriminate species using phenological variation in their reflectance spectra, but also that tree species can be better differentiated by also using LiDAR-derived structural and intensity properties (for a detailed review, see Fassnacht et al. 2016). Here, we take advantage of both spectral and structural properties to help quantify and better understand how passive and active remote sensing data can improve discrimination of tree species at the individual crown-level.

Using multi-temporal data to capture different phenological patterns is a widely used approach for tree species discrimination (Key et al. 2001; Madonsela et al. 2017; Reed et al. 1994; Wolter et al. 1995). By incorporating seasonal variation in the biochemical, physiological and structural properties of tree crowns, spectral variation linked to phenology has been adopted for many different remote sensing applications, including climate interactions (e.g. He et al. 2015), land cover assessment (Ganguly et al. 2010), crop observation (Sakamoto et al. 2005) and tree species mapping (Reed et al. 1994). However, at high spatial resolutions, it is challenging to obtain satisfactory images that capture phenological patterns for differentiating individual trees for an entire growing season (Reed, Schwartz, and Xiao 2009). A number of studies have therefore used a variety of sensors to capture the most striking seasonal characteristics (Voss and Sugumaran 2008; Wolter et al. 1995). Studies involving multi-temporal datasets generally conclude that the most informative image acquisition times are often in short windows surrounding the spring green-up period, peak summer, and autumn senescence phenology periods (Hill et al. 2010; Key et al. 2001; Klosterman et al. 2014; Voss and Sugumaran 2008; Wolter and Townsend 2011).

A key advantage of LiDAR for tree species discrimination is its ability to measure three-dimensional features useful for delineating tree crowns and describing species differences in crown architecture and structure (Alonzo, Bookhagen, and Roberts 2014; Brandtberg 2007; Dalponte, Bruzzone, and Gianelle 2008; Dalponte et al. 2013; Fang et al. 2016; Ghosh et al. 2014; Heinzl and Koch 2011; Kim 2007; Liu, Im, and Quackenbush 2015; Vaughn, Moskal, and Turnblom 2012). For tree species classification, some studies have also recognized the value of combining LiDAR and multispectral data. Especially due to the complexity of tree crowns and similarity of spectral features between species, height information from LiDAR is often the most important factor to improve discrimination performance (Alonzo, Bookhagen, and Roberts 2014; Dalponte, Bruzzone, and Gianelle 2008; Jones, Coops, and Sharma 2010). LiDAR is also increasingly being used to link structural and spectral information in the form of the intensity of returns, which is related to the reflecting object's spectral reflectance and the proportion of the laser beam cross-section that intersects with that object (Brandtberg 2007; Eitel et al. 2016; Fassnacht et al. 2016). LiDAR intensity provides invaluable information on species differences in crown architecture, thereby increasing differentiation of tree species (Brandtberg et al. 2003). For instance, broadleaf trees and conifers can be distinguished by LiDAR intensity values because coniferous tree architectures scatter more infrared light downward into their crowns, and thus provide a lower intensity value compared with broadleaved trees (Kim 2007; Knyazikhin et al. 2013; Vauhkonen et al. 2014). Intensity also differs within

functional groups; for needleleaf evergreen trees, Holmgren and Persson (2004) found that the mean intensity is higher for Norway spruce (*Picea abies* L. Karst) trees, with a higher standard deviation of intensity due to denser leaves, compared with Scots pines. Nevertheless, a full understanding of LiDAR intensity for species discrimination (Fassnacht et al. 2016; Korpela et al. 2010), and its potential, especially relative to other spectral and structural information, warrants further evaluation.

The primary goal for this study is to evaluate the utility of combining (a) high spatial resolution multispectral images from three different phenological stages, and (b) height and intensity data from leaf-on LiDAR data, to classify tree species at the individual crown level with a machine learning classifier at the Fernow Experimental Forest (FEF), West Virginia. We hypothesize that each of these image datasets will improve the separability of tree species, and add meaningful biophysical information, thereby enhancing the ability to discriminate tree species remotely.

Our approach assumes a geographic object-oriented (GEOBIA) framework for tree-species classification (Warner et al. 1999). From each tree crown polygon, we extract six groups of variables, including spectral reflectance information from optical imagery that captures (1) spring, (2) summer, and (3) autumn phenology, (4) height and intensity data from leaf-on (peak summer) LiDAR, as well as (5) spectral indices and (6) texture information derived from the first four groups of variables. Then, we evaluate the relative performance of these groups of variables in Random Forest (RF) classification models. We also use analysis of variance (ANOVA) and decision trees to help understand how the LiDAR and phenological variables work individually, as well as work together to identify the distinct spectral and structural properties of each tree species. Together, these approaches are designed to help test how combinations of variables can provide a more robust method for measuring a fuller suite of spectral, phenological, and crown architectural differences useful for discriminating tree species with remotely sensed data.

2. Methods

2.1. Study area

Our study site includes two unmanaged reference compartments within the United States Department of Agriculture (USDA) Forest Service's Fernow Experimental Forest (FEF), located in Tucker County, West Virginia (Figure 1: 39°3'15"N, 79°41'15"W). The topography within each of these roughly 40 ha compartments is steeply sloped with elevations ranging between 762 and 854 m (Burnham et al. 2017). The forests have been unmanaged following an almost complete harvest in the 1920's. Mean annual precipitation is approximately 1450 mm and mean annual temperature is 9.2°C. The dominant tree species are red oak (*Quercus rubra*), sugar maple (*Acer saccharum*), tulip poplar (*Liriodendron tulipifera*), and black cherry (*Prunus serotina*). Other species include American basswood (*Tilia Americana*), black birch (*Betula lenta*), chestnut oak (*Quercus prinus*), cucumber magnolia (*Magnolia acuminata*), frasier magnolia (*Magnolia fraseri*), red maple (*Acer rubrum*), shagbark hickory (*Carya ovata*), white ash (*Fraxinus americana*) and white oak (*Quercus alba*).

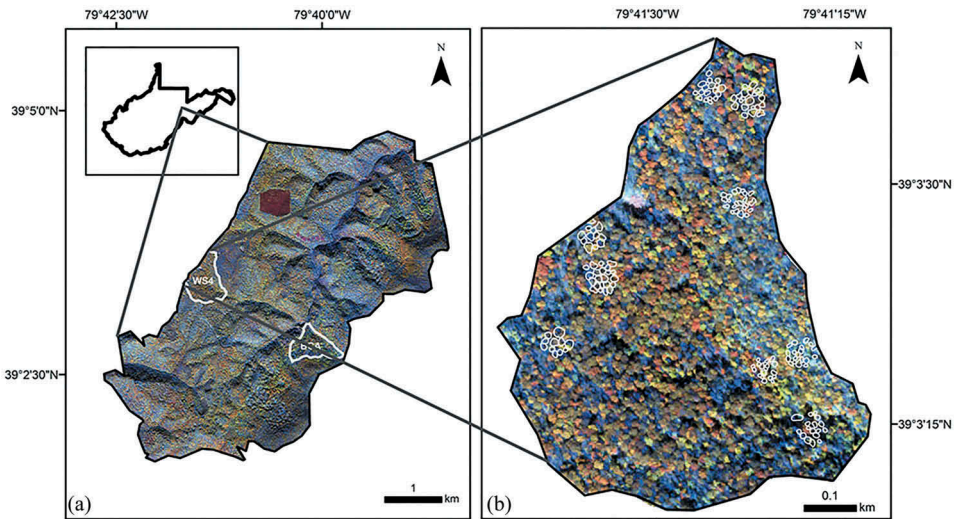


Figure 1. Study site at the Fernow Experimental Forest (a), WV, USA, showing a portion of the delineated tree crowns (White polygons) in the Watershed #4 (WS4) reference compartment (b). The background image illustrates tree crown differences in the autumn phenology by displaying Worldview-2 bands Red edge, Yellow, Blue in the red, green, and blue (RGB) colour channels. We use the yellow and red edge bands here because they are effective in capturing autumn phenology.

2.2. Methods overview

Our general workflow included a field survey, manual delineation of individual crown polygons, data preprocessing, feature extraction, feature selection and grouping using Random Forests to evaluate the relative performance of feature groups, and finally, using decision trees and ANOVA to evaluate data combinations (Figure 2).

2.3. Field measurements

We completed all the field mapping of tree crowns during May 2015 using 0.2 hectare (0.5 acre) circular permanent forest plots within the two selected reference compartments at the Fernow: watershed 4 (WS 4) and the biological control area (BCA) (Figure 1). For each tree reaching the canopy in these plots, we recorded the species name, diameter at breast height (DBH), and tree height as measured with a Nikon Forestry Pro Laser Rangefinder. We also used the laser range finder to precisely map the distance and bearing of each stem from the plot centroids. We recorded the location of all centre points with a survey grade post-processed GPS unit (<0.5 m error). Following these measurements, we hand-sketched the crown extents of each mapped tree to aid our manual crown delineation process conducted with the imagery datasets.

2.4. Imagery datasets

The LiDAR data were collected on 20 July 2014 using an aircraft flying at 915 m with an average speed of 250 km hour⁻¹, and an Optech ALTM 3100 LiDAR sensor with a pulse rate frequency of 100 kHz. Intensity data from this sensor's near-infrared laser beam has

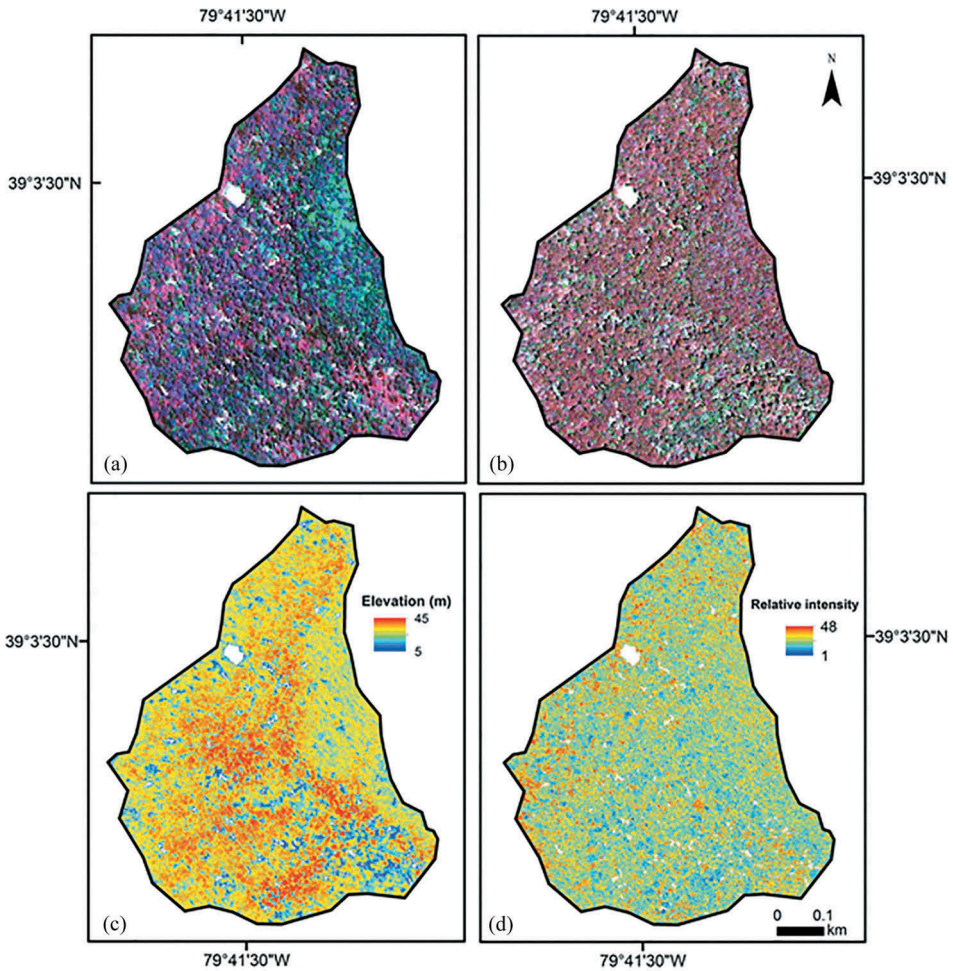


Figure 2. The Fernow Watershed #4 portion of the study area. (a) Spring image. (b) Summer image. (c) LiDAR canopy height model. (d) LiDAR intensity. (a) and (b) are standard false colour infrared composites (bands NIR, Red, Green displayed as RGB). In each image, pixels with a canopy height less than 5 m are masked (and displayed in white) in order to highlight the variability among intact canopies. Compare to [Figure 1](#), which shows the autumn phenology image.

been found to correlate strongly with measured spectral reflectance at the laser's 1064 nm wavelength (Ahokas et al. 2006; Vain et al. 2009). The LiDAR data, collected with > 50% overlap between flight-lines, provided an average of 6.6 returns m^{-2} . We focused on LiDAR variables that are routinely calculated using standard GIS and remote sensing software in a raster environment. First-return data were rasterized to produce a Digital Surface Model (DSM), and last returns to produce a Digital Elevation Model (DEM). Rasterization was done in ArcMap 10.5 with a common 0.5 m cell size by assigning the average of all points within a cell as the elevation and linear interpolation as void fill method. We created a Canopy Height Model (CHM) from the difference between the DSM and the DEM. We rasterized the LiDAR intensity data using all the returns in each 0.5 m pixel.

We selected three high-resolution satellite images to best characterize phenological differences among species (Figures 1 and 3 and Table 1). Visual inspection of the images indicates that the image dates correspond to three key phenology phases within broad-leaf deciduous forests: the leaf emergence and flowering phase of spring (Figure 3(a)), the full-canopy development of summer (Figure 3(b)), and the leaf senescence and abscission of autumn (Figure 3(c)). All three sensors, GeoEye, Pleiades and WorldView2 provide approximately 2 m multispectral (MS) bands, as well as an approximately 0.5 m panchromatic band. Our spring and summer images have four MS bands, and the autumn image has eight bands (Table 2).

2.5. Image pre-processing

We separately registered the multispectral and panchromatic images to the base layer of the LiDAR Canopy Height Model using Erdas Imagine 2016 and ArcMap 10.5. We applied a rational polynomial coefficient (RPC) sensor model (Toutin 2004) with elevation information and with ground control points (GCPs) to achieve a low RMSE (<1 pixel) for image registration (Supplemental data, Table S1). Next, for each GeoEye, Pleiades and WorldView 2 multispectral and panchromatic band, we used the image metadata (IMD file) to convert digital numbers to ground reflectance using the CosT approach (Chávez 1996).

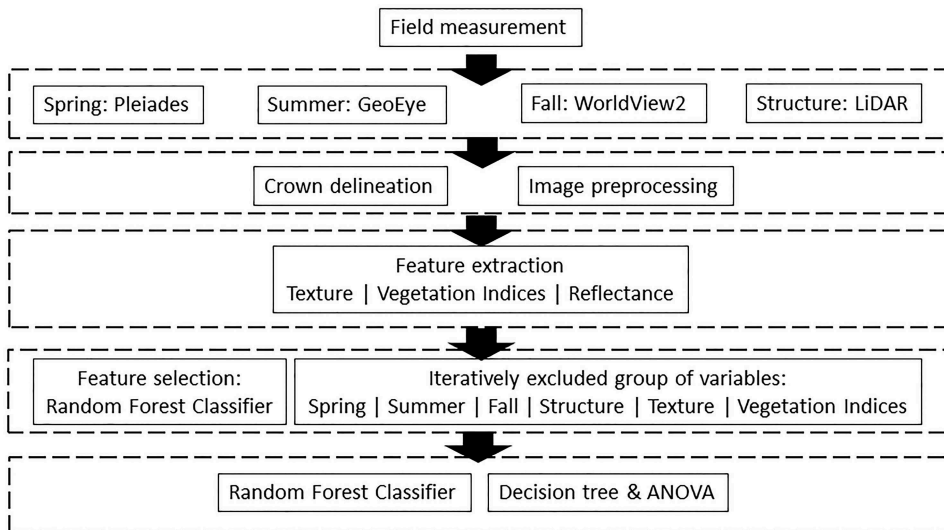


Figure 3. Flowchart of identifying tree species in FEF.

Table 1. Metadata of the imagery used in the study.

Sensor	Acquisition date	Phenological period	Off-nadir view angle (°)	Pan band resolution (m)	Multispectral band resolution (m)
LiDAR	20 July 2014	Summer	0–25		
GeoEye	6 June 2014	Summer	8.0	0.42	1.67
Pleiades	15 May 2015	Spring	20.6	0.70	2.80
WorldView2	26 October 2014	Autumn	26.7	0.57	2.28

Table 2. Image band wavelengths.

Sensor	Wavelength (nm)									
	Pan	Coastal	Blue	Green	Yellow	Red	Red Edge	NIR1	NIR2	LiDAR laser
LiDAR										1064
GeoEye	450–800		450–510	510–580		655–690		780–920		
Pleiades	470–830		430–550	500–620		590–710		740–940		
WorldView2	450 – 800	400 – 450	450–510	510 – 580	585 – 625	630–690	705–745	770–895	860–1040	

2.6. Crown delineation using field and imagery data

The focus of this work is on object-based classification. In this paper, we only explore the issue of classification, and not errors due to segmentation issues (Liu and Xia 2010). Therefore, we used manually delineated crown polygons to ensure the highest accuracy in the segmentation. We visually compared tree crown field maps with high-resolution LiDAR height data, as well as panchromatic data layers from the spring, summer, and autumn images. From these data sources, we manually delineated the non-overlapping polygons as 267 mapped tree crowns. In our analysis, we only attempt to discriminate crowns from the four most abundant tree species. Thus, our analysis dataset includes 57 red oak, 32 sugar maple, 26 tulip poplar, and 20 black cherry crowns for a total of 135 total tree crowns.

2.7. Variable extraction

By computing the zonal average within each delineated tree crown, we extracted six groups of variables (Table 3): spectral reflectance from all multispectral bands in the (1) spring, (2) summer, and (3) autumn images, (4) vegetation indices derived from the three multispectral datasets, (5) canopy height and intensity from the LiDAR imagery, and (6) texture related variables from the panchromatic and LiDAR datasets. For vegetation indices, we computed the normalized difference vegetation index (NDVI) using the red and NIR multispectral bands from the spring, summer and autumn images. Using the eight spectral bands of WorldView 2 imagery, we also calculated additional vegetation indices on the autumn image: red edge and yellow band ratio (Waser et al. 2014), plant senescence index (Omer et al. 2016), NIR and yellow band ratio (Waser et al. 2014) and enhanced vegetation Index (EVI) (Omer et al. 2016) (Table 3).

Textural characteristics may vary based on several aspects of crown architecture that may differ among species, including internal shading, leaf orientation, as well as leaf density and size (Sayn-Wittgenstein 1978). We used the panchromatic reflectance of the spring, summer, and autumn images, as well as LiDAR height and intensity data layers, to compute four types of texture variables (Haralick, Shanmugam, and Dinstein 1973) based on the grey-level co-occurrence matrices (GLCM). The texture was calculated within eCognition. The eCognition GLCM texture averages the four directions 0°, 45°, 90°, 135° at an offset of 1 pixel (Trimble 2011). The four texture features are as follows: (1) Homogeneity, which describes the similarity of pixel values within the local region; a high value indicates a more homogeneous region. (2) Contrast, which summarizes the variation of pixel values and a high value indicates a locally more heterogeneous region. (3) Entropy, which is a measure of the disorder or randomness in the image values. (4) Dissimilarity, which is a measure of the heterogeneity of pixel values within the local region (Warner 2011).

Table 3. Variables used in the analysis.

Group	Feature name	Description*	Sensor/source	Reference	
Spectral reflectance	Reflectance 1–4	Average reflectance band 1–4	GeoEye	Pu and Landry (2012)	
	Reflectance 1–4	Average reflectance band 1–4	Pleiades		
	Reflectance 1–8	Average reflectance band 1–8	WorldView2		
	Brightness 1–3	Mean value of the means of all bands	GeoEye, Pleiades and WorldView 2		
	Reflectance panchromatic band 1–3	Average panchromatic reflectance	GeoEye, Pleiades and WorldView 2		
LiDAR	Height	Average height	LiDAR CHM	Waser et al. (2014)	
	Intensity	Average intensity	LiDAR intensity image		
Vegetation indices	RedEdge yellow ratio	$(R_{\text{RedEdge}} - R_{\text{Yellow}})/(R_{\text{RedEdge}} + R_{\text{Yellow}})$	WorldView 2	Omer et al. (2016)	
	Plant Senescence 1	$(R_{\text{Red}} - R_{\text{Blue}})/R_{\text{NIR1}}$	WorldView 2	Waser et al. (2014)	
	Plant Senescence 2	$(R_{\text{Red}} - R_{\text{Blue}})/R_{\text{RedEdge}}$	WorldView 2	Waser et al. (2014)	
	NIR yellow ratio	$(R_{\text{NIR2}} - R_{\text{Yellow}})/(R_{\text{NIR2}} + R_{\text{Yellow}})$	WorldView 2	Waser et al. (2014)	
	NDVI WW2	$(R_{\text{NIR}} - R_{\text{Red}})/(R_{\text{NIR}} + R_{\text{Red}})$	WorldView2	Karlsson 2016	
	NDVI P	$(R_{\text{NIR}} - R_{\text{Red}})/(R_{\text{NIR}} + R_{\text{Red}})$	Pleiades	Omer et al. (2016)	
	NDVI G	$(R_{\text{NIR}} - R_{\text{Red}})/(R_{\text{NIR}} + R_{\text{Red}})$	GeoEye		
	EVI	$2.5 \times ((R_{\text{NIR1}} - R_{\text{Red}})/(R_{\text{NIR1}} + 6 \times R_{\text{Red}} - 7.5 \times R_{\text{Blue}} + 1))$	WorldView 2	Pu and Landry (2012)	
	Texture	GLCM homogeneity	GLCM homogeneity	Panchromatic band of WorldView 2, Pleiades, GeoEye; and LiDAR CHM and intensity	Pu and Landry (2012)
		GLCM contrast	GLCM contrast	Panchromatic band of WorldView 2, Pleiades, GeoEye; and LiDAR CHM and intensity	
GLCM entropy		GLCM entropy	Panchromatic band of WorldView 2, Pleiades, GeoEye; and LiDAR CHM and intensity		
GLCM dissimilarity		GLCM dissimilarity	Panchromatic band of WorldView 2, Pleiades, GeoEye; and LiDAR CHM and intensity		

*Where *R* is the reflectance and the subscript refers to the spectral band (e.g. Blue, Red, etc.).

In total, we extracted 52 variables for each individual crown. These include 11 variables from the spring Pleiades image, 11 variables from the summer GeoEye image, 20 variables from the autumn WorldView2 image (Extra variables from WorldView2 were calculated from four additional bands compared with GeoEye) and 10 variables from LiDAR (Table 3).

2.8. Data analysis

To avoid problems due to the ‘curse of dimensionality’ (Hughes 1968) associated with discriminating 4 species from 52 variables, we selected the best subset of variables before classification in R (R Core Development Team 2016). We used *rfUtilities* package (Evans and Murphy 2014) to select variables based on variable importance. We used *caret* package (Kuhn et al. 2016) to run a step-wise RF with the best 10%, 15%, 25%, 50%, 75%, and 90% of the variables retained. We generated 500 trees for each RF model. Based on prior experience which suggested any number greater than 100 was sufficient; we used 500 to be sure the number was large enough. The optimal number of variables available for splitting at each node (*mtry*) was selected using 10-fold cross-validation and ten different values were assessed. This 10-fold cross validation randomly split data into 10 subsets; 9 of them are used for training and 1 retained for testing each time. The average was calculated in the model as final accuracy (Maxwell, Warner, and Fang 2018). From this, we selected the top 50% of the variables as the greatest per cent that retained the most signal while minimizing redundancy and noise. The cross-fold validation approach was used so that classification trains a classifier with a number of samples that is similar to the number of variables. Accuracy could be evaluated based on data entirely separate from that used in developing the model. RF does offer estimates of accuracy based on data withheld from subsets of the model used in developing the trees (so-called out of bag estimates), but we prefer to use entirely separate data for both overall accuracy assessment and the confusion matrices (Maxwell, Warner, and Fang 2018). Using the six groups of variables described in Section 2.6, we conducted a preliminary test to evaluate the accuracy of RF models that only drew from an individual group of variables (see Figure S1 and Table S2 in the supplemental material). As we expected, the Kappa values obtainable from a single group were markedly lower than combining groups, so we focused the remainder of our analysis on testing our hypotheses concerning the combination of spectral features with structural features to enhance tree species discrimination.

To test how each group of variables enhanced model accuracy, we iteratively removed each of the six groups of variables and recorded the effect on the Kappa value derived from the 10-fold cross-validation of the RF model. These RF models used 31 features with spring image variables excluded, 31 features with summer image variables excluded, 21 features with autumn image variables excluded, 32 features with LiDAR variables excluded, 30 features with texture features excluded, and 32 features with vegetation indices excluded. Finally, in order to understand the patterns and mechanisms of how the variables used in the RF modelling are useful individually and in combination for discriminating tree species, we used ANOVA (assumptions tested in Supplemental data, Table S3), paired *t*-tests, and unpruned decision trees generated in R with the *rpart* package (Therneau, Atkinson, and Ripley 2017). An ANOVA test can

help to test the difference among group means with the hypothesis that the group means are equal. F -ratio is the ratio of between groups to within-group variance. Group means are significantly different when the p -value (significance) is less than 0.05 and F -ratio is larger than 1.

A single decision tree classification tends to be less accurate than RF, which employs an ensemble of trees (Maxwell, Warner, and Fang 2018). Nevertheless, the single decision tree has the advantage of being simple and intuitive to interpret. Because our main aim in this study was to explore the importance of different data layers, a decision tree classification is therefore used as a supplement to the RF classification. The decision tree classification was carried out with the `rpart` package (Therneau, Atkinson, and Ripley 2017). The tree was automatically pruned based on $cp = 0.01$, $minsplit = 20$, $maxcompete = 4$.

3. Results

3.1. Data combinations and random forest model accuracy

The Random Forest model achieved a Kappa value of 42.4% (with an overall accuracy (OA) of 62%) when we ran it with the top 50th percentile of all the variables from all groups. Notably, the variables in this top 50th percentile were drawn from each of the six groups of variables (Table 4). When we iteratively excluded groups of variables, we found that removing each group caused a notable decrease in Kappa value compared with results from a full model (Figure 4). Removing variables from the summer GeoEye image caused the largest percentage (6.1%) drop in Kappa value, from 42.4% with the full model to 36.3%. The LiDAR variables were the next most useful group of variables, reducing Kappa by 5.1% when they were excluded. The four other groups of variables all caused smaller decreases in Kappa value, but still reduced model performance considerably. The overall magnitude of reduced performance in these four other groups was between 2.3% and 3.9% in terms of Kappa value, corresponding to a 5–10% relative reduction in the model performance in comparison to the full model.

The confusion matrix from RF using the top 50th percentile of variables indicates that the sample size of each species likely influenced the results. Red oak ($N = 57$ crowns) had the largest producers (PA) and users accuracy (UA), while black cherry ($N = 20$ crowns) had the lowest accuracy (Table 5). Confusion matrices from other RF models highlight substantial drops in accuracy for individual species when certain of groups of variables were withheld (Supplemental data, Table S4). This was especially evident for sugar maple, which fell from a 58% UA and 48% PA in the 50th percentile RF model to a 40% UA and 31% PA in the model with the LiDAR data withheld (Supplemental data, Table 4(b)).

3.2. Useful variables identified by ANOVA and a decision tree

ANOVA analyses revealed that LiDAR intensity had the strongest individual ability to discriminate tree species (Table 4), and further analysis using pair-wise t -tests revealed that sugar maple had significantly higher intensity than other species (Figure 5(a)). Reflectance in the blue wavelengths during the spring and summer was among the next strongest variables (Table 4), and t -tests revealed that red oak crowns had lower

Table 4. Features selected by random forest, feature selection sorted by decreasing *F*-value obtained from ANOVA tests of species differences.

Feature name	Significance ^a	<i>F</i> -ratio	Variable groups ^b
Average intensity	< 0.001	10.1	LI
Spring blue reflectance	< 0.001	9.22	SP
Summer NDVI	< 0.0001	9.02	SU&VI
Spring NDVI	< 0.0001	8.20	SP&VI
Spring NIR reflectance	< 0.0001	7.93	SP
Summer red reflectance	< 0.001	7.75	SU
GLCM entropy of intensity	< 0.0001	7.72	LI&TE
Summer blue reflectance	0.0002	7.20	SU
Autumn GLCM entropy	0.0002	7.16	AU&TE
Spring GLCM entropy	0.0002	7.11	SP&TE
Spring green reflectance	0.0003	6.79	SP
Spring Brightness	0.0003	6.79	SP
Summer GLCM entropy	0.0005	6.33	SU&TE
LiDAR GLCM entropy	0.0013	5.53	LI&TE
Autumn blue reflectance	0.0020	5.21	AU
Autumn Plant Senescence	0.0022	5.13	AU &VI
Autumn NIR and yellow ratio	0.0031	4.84	AU &VI
Autumn coastal reflectance	0.0033	4.81	AU
Autumn Red Edge and yellow ratio	0.0075	4.16	AU &VI
Autumn NIR2 reflectance	0.0096	3.96	AU
Autumn red reflectance	0.0108	3.88	AU
NIR1 reflectance	0.0130	3.73	AU
Spring red reflectance	0.0140	3.67	SP
Autumn Brightness	0.0172	3.51	AU
Autumn NDVI	0.0218	3.33	AU &VI
Autumn Enhanced vegetation index	0.0269	3.16	AU &VI
Autumn Red Edge reflectance	0.0343	2.97	AU
LiDAR GLCM homogeneity	0.0346	2.96	LI&TE
Autumn Panchromatic reflectance	0.0406	2.84	AU
Spring Panchromatic reflectance	0.0427	2.8	SP
LiDAR Tree height	NS	2.58	LI
Intensity GLCM contrast	NS	1.76	LI&TE
Intensity GLCM dissimilarity	NS	1.59	LI&TE
Autumn yellow reflectance	NS	1.32	AU
Summer NIR reflectance	NS	1.23	SU
Summer GLCM dissimilarity	NS	0.79	SU&TE
Summer Brightness	NS	0.63	SU
Autumn green reflectance	NS	0.52	AU
Autumn GLCM homogeneity	NS	0.13	AU &TE

^aNS: not significant^bSP: Spring; SU: Summer; AU: Autumn; LI: LiDAR; TE: Texture; VI: Vegetation indices

summer blue reflectance and higher spring blue reflectance (Figure 5(b, c)). The vegetation indices also proved to be useful variables (Table 4), particularly the plant senescence index which indicated a notably higher index value for tulip popular during the autumn phenology image acquisition (Figure 5(d)).

Most of these useful variables were also selected by the decision tree analysis. The most parsimonious decision tree used 8 variables. As with the RF model, the decision tree notably contained variables derived from each of the four image datasets (spring, summer, autumn, and leaf-on LiDAR) (Figure 6). Summer blue reflectance was the initial node, followed by blue and brightness bands from the spring image. Three spectral indices describing species differences in the autumn senescence, and two LiDAR variables describing differences in intensity and entropy of height provided the final nodes discriminating all four species (Figure 6).

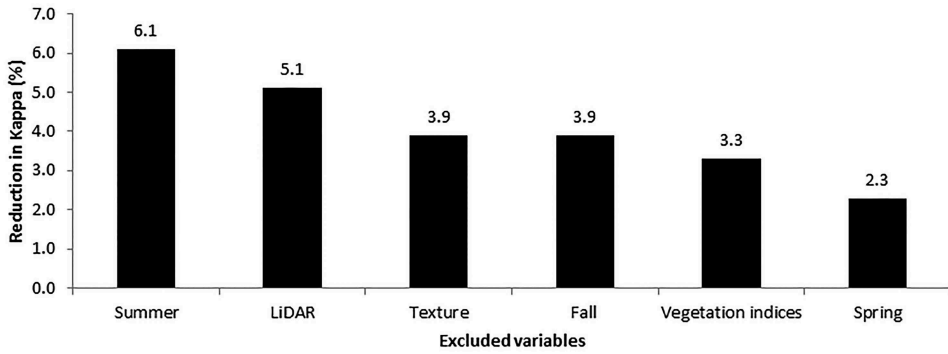


Figure 4. Per cent of Kappa value lost by removing each group of variables.

Table 5. Confusion matrix from RF classification of individual trees with top 50th percentile of variables.

Classification	Reference				Total	UA (%)
	Black cherry	Red oak	Sugar maple	Tulip poplar		
Black cherry	2	0	1	1	4	50
Red oak	10	50	14	5	79	63
Sugar maple	3	5	15	3	26	58
Tulip poplar	5	2	2	17	26	65
Total	20	57	32	26	135	
PA (%)	10	88	47	65		

OA (%) = 62

PA: Producer's accuracy; UA: User's accuracy; OA: Overall accuracy

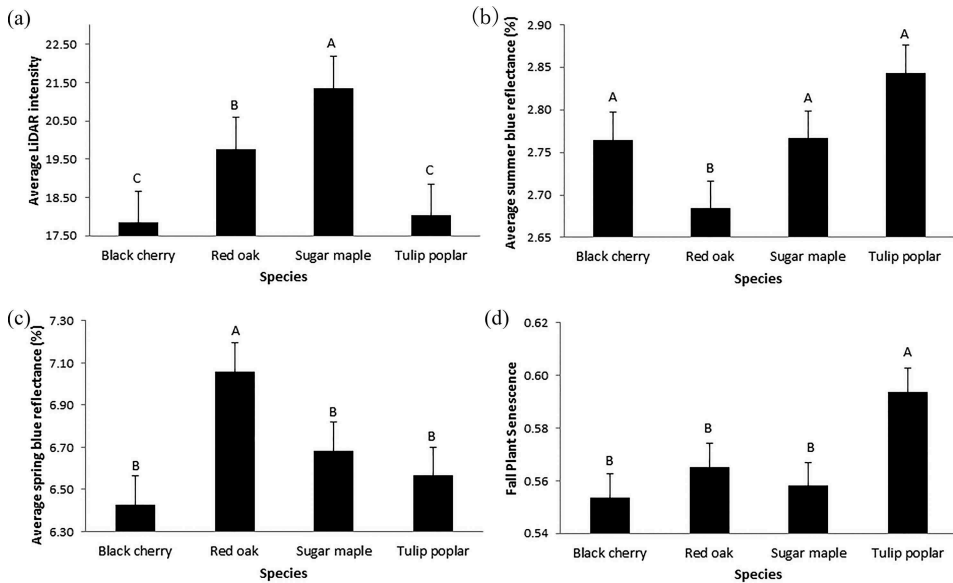


Figure 5. Key results from the ANOVA tests, letters denote significant differences in means, as assessed by pair-wise t-tests.

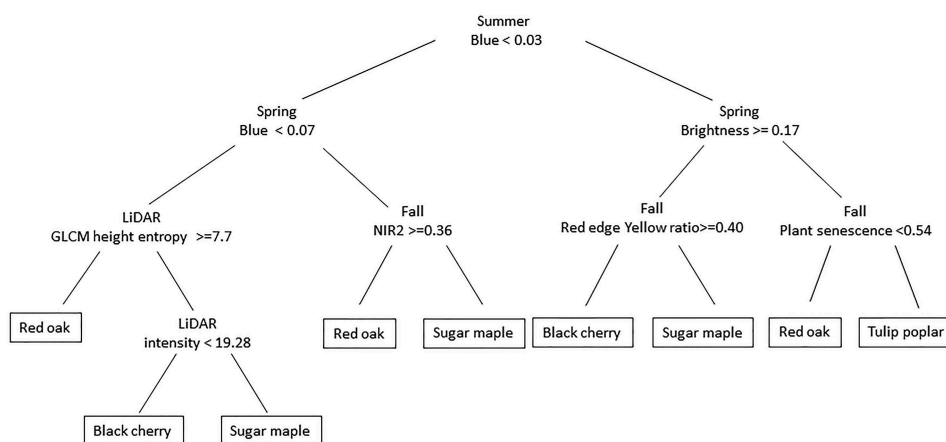


Figure 6. Decision tree based on 50th percentile of variables. Affirmative logical decisions are in each case to the left.

4. Discussion

Our results strongly support the hypothesis that the combination of phenology and structural information from individual tree crowns can enhance the discrimination of tree species. First, our RF results supported the hypothesis that each group of variables would enhance model performance (Figure 4). Our separate analysis using decision trees supported this combination because all three phenology images and LiDAR were included in the most parsimonious decision tree (Figure 6). However, the relative degree to which the groups of variables affected model accuracy differed from some previous studies. For instance, whereas we found the summer and spring phenology periods to contain the most useful variables for species discrimination (Figure 4), others have found a peak autumn image to be most useful (e.g. Key et al. 2001). Even so, reflectance and spectral indices from the autumn image were selected by RF (Table 3), and also formed key parts of the decision tree analysis (Figure 6). Thus, our data still indicate strong support for including autumn phenology in species discrimination methods. The RF analysis also indicated that LiDAR-derived variables were the second most useful group of variables, which adds support to a growing number of studies emphasizing the importance of LiDAR information for tree species classification (Dalponte, Bruzzone, and Gianelle 2008; Donoghue et al. 2007; Eitel et al. 2016; Ghosh et al. 2014; Jones, Coops, and Sharma 2010; Kim 2007; Korpela et al. 2010; Voss and Sugumaran 2008).

Our ANOVA and decision tree analyses suggest several mechanisms by which spectral and structural information help discriminate broadleaf deciduous tree species based on their unique phenology and crown architectural traits. Specifically, the spectral information in the visible wavelengths helps to describe the unique phenology of leaf pigments and photosynthetic activity in each tree species, while the phenology of NIR spectral reflectance and LiDAR describe essential species differences in tree crown architecture (Asner 1998; Eamus, Huete, and Yu 2016; Gates et al. 1965; Mohammed et al. 2000; Ollinger 2011; Rautiainen et al. 2004). First, our observations that red oak has a high spring blue reflectance (Figure 5(c)), low

summer blue reflectance (Figure 5(b)), and a high autumn NIR reflectance (Figure 6) matches with field observations that red oak crowns tend to have a later leaf emergence in the spring, grow dense crowns of photosynthetically active leaves in the summer, and senesce later in the autumn relative to other species. High GLCM entropy of height as indicated by the decision tree differentiation of red oaks (Figure 6) suggests that red oak has relatively more within-crown gaps than other species. Next, a higher plant senescence index for tulip poplar (Figure 6) matches field observations of an earlier autumn leaf senescence in tulip poplar than other species (particularly red oak). Finally, coupled with observations of its lower entropy of height, observations of high summer LiDAR intensity (Figures 5(a) and 6) indicate that sugar maple has a flatter and more horizontal crown architecture (Budei et al. 2018; Fassnacht et al. 2016; Kim et al. 2009). The importance of LiDAR for characterizing this unique crown architecture of sugar maple was borne out by the large drop in classification accuracy when LiDAR variables were removed from the RF model (Table 4 and Supplemental data Table 3 (b)).

Although the overall accuracies obtained in this study were lower than might be useful for mapping purposes, we emphasize that the ultimate purpose of this study was to provide guidance in data selection for future mapping, and not necessarily to produce a map directly from these data (see, for example, Key et al. 2001, for a similar research design). Indeed, the strong complementarity of spectral and structural information in our study illustrates how the combination of LiDAR and multi-temporal images can contribute to tree species discrimination, especially in forests where trees have similar functional types and reflectance characteristics (Alonzo, Bookhagen, and Roberts 2014; Dalponte, Bruzzone, and Gianelle 2008; Jones, Coops, and Sharma 2010). Yet, the overall accuracy of our discrimination algorithm ($Kappa = 42\%$) highlights that substantial obstacles still remain toward an ultimate goal of automatic crown-level species discrimination from remotely sensed data. Our study exemplifies the challenge of these obstacles. First, our study design relied on available archived data. While we were able to match archive data to key phenology periods, it was challenging to precisely co-register the images that had less than ideal viewing geometries (Table 1), and were collected over a topographically complex study site. Second, study areas like the Fernow Experimental Forest are especially challenging for discriminating tree species because the trees (1) have similar growth forms, leaf types and leaf habits, and (2) have high within-species variance in phenology and crown architecture linked to strong competition for light within a diverse forest on steeply sloping terrain. Given these unique characteristics of our study design and study area, we suggest that our classification accuracy and evidence of data combination are quite conservative results. As such, in more forgiving study contexts, we would expect substantially higher accuracies and even stronger evidence for the advantage of combinations of multispectral and LiDAR data.

5. Conclusion

The significant contribution of this paper is that combining multi-temporal imagery with leaf-on LiDAR can enhance the ability to discriminating tree species based on their phenology and crown architectural characteristics. Specifically, our results reveal that the combination of multi-temporal high-resolution images with leaf-on LiDAR data improves

the discrimination of four broadleaf deciduous tree species: red oak, sugar maple, black cherry and tulip poplar. We tested six groups of variables for their classification performance: (1) spring, (2) summer, and (3) autumn phenology, (4) height and intensity data from leaf-on LiDAR, (5) spectral indices and (6) texture information. When a specific group of variables was removed, the decrease in Random Forest classification accuracy demonstrates the importance of such variables. In addition, our ANOVA and decision tree results illustrate specific mechanisms to discriminate species based on their unique phenology and crown architectural properties. Continuing to build on these findings can provide a robust path toward the ultimate goal of automatic crown-level tree species discrimination.

The RF classification indicated that the Kappa value dropped each time a specific group of variables was removed. This strongly indicates all three seasons of high-spatial resolution multi-temporal satellite data and leaf-on LiDAR enhanced the ability to discriminate tree species. We find that summer phenology is most helpful to classify tree species since our model is most affected (declined in Kappa accuracy of 6.1%) by removing summer phenology features. Crown structural and architecture features from LiDAR were the second-best variables for discriminating tree species. Next, texture features, fall phenology and vegetation indices showed similar importance for tree species classification. Variables from a spring image were the least helpful to classify tree species, but they still cause 2.3% drop in Kappa value when excluded.

The decision tree and ANOVA results provide additional evidence regarding how these imagery sources combine to identify the distinct spectral and structural properties for each tree species. We found blue band reflectance from multi-temporal remote sensing imagery to be a useful variable in describing unique phenological and structural features associated with leaf emergence. Autumn NIR may be important for capturing differences for red oak associated with leaf senescence. Moreover, for crown architectural properties, relative lower summer blue reflectance indicates dense crowns; higher entropy of height suggests more within-crown gaps in red oak. In another abundant species, sugar maple, we also found that higher summer LiDAR intensity corresponds with flatter crown architecture (Lower height entropy). Thus, for discriminating broadleaf deciduous tree species, this study supports the utility of high spatial multi-temporal satellite images in the spring, summer and fall to capture the most distinctive phenology patterns while also supporting the use of leaf-on LiDAR for capturing key differences in tree crown architecture.

Acknowledgments

We are grateful for generous funding from West Virginia University, the USDA Forest Service, and the NASA West Virginia Space Grant programs. We thank Paul Kinder, Dan Miller, Brian Mills, and Adam Riley for their expertise with the LiDAR data collection, Lindsay Deel for help with pre-processing the summer GeoEye image, as well as Mary Beth Adams and the Fernow Experimental Forest staff for help with the field mapping and access to the permanent growth plots.

Disclosure statement

No potential conflict of interest was reported by the authors.

ORCID

Fang Fang  <http://orcid.org/0000-0001-7541-189X>

Timothy A. Warner  <http://orcid.org/0000-0002-0414-9748>

References

- Ahokas, E., S. Kaasalainen, J. Hyypä, and J. Suomalainen. 2006. "Calibration of the Optech ALTM 3100 Laser Scanner Intensity Data Using Brightness Targets." *International Archives of Photogrammetry, Remote Sensing and Spatial Information Sciences*, 36, A1, CD-ROM.
- Alonzo, M., B. Bookhagen, and D. A. Roberts. 2014. "Urban Tree Species Mapping Using Hyperspectral and Lidar Data Fusion." *Remote Sensing of Environment* 148: 70–83. doi:10.1016/j.rse.2014.03.018.
- Asner, G. P. 1998. "Biophysical and Biochemical Sources of Variability in Canopy Reflectance." *Remote Sensing of Environment* 64 (3): 234–253. doi:10.1016/S0034-4257(98)00014-5.
- Brandtberg, T. 2007. "Classifying Individual Tree Species under Leaf-Off and Leaf-On Conditions Using Airborne Lidar." *ISPRS Journal of Photogrammetry and Remote Sensing* 61 (5): 325–340. doi:10.1016/j.isprsjprs.2006.10.006.
- Brandtberg, T., T. A. Warner, R. E. Landenberger, and J. B. McGraw. 2003. "Detection and Analysis of Individual Leaf-Off Tree Crowns in Small Footprint, High Sampling Density Lidar Data from the Eastern Deciduous Forest in North America." *Remote Sensing of Environment* 85 (3): 290–303. doi:10.1016/S0034-4257(03)00008-7.
- Budei, B. C., B. St-Onge, C. Hopkinson, and F. A. Audet. 2018. "Identifying the Genus or Species of Individual Trees Using a Three-Wavelength Airborne Lidar System." *Remote Sensing of Environment*. doi:10.1016/j.rse.2017.09.037.
- Burnham, M. B., J. R. Cumming, M. B. Adams, and W. T. Peterjohn. 2017. "Soluble Soil Aluminum Alters the Relative Uptake of Mineral Nitrogen Forms by Six Mature Temperate Broadleaf Tree Species: Possible Implications for Watershed Nitrate Retention." *Oecologia* 185 (3): 327–337. doi:10.1007/s00442-017-3955-8.
- Chávez, P. S. Jr. 1996. "Image-Based Atmospheric Corrections - Revisited and Improved." *Photogrammetric Engineering and Remote Sensing* 62 (9): 1025–1036.
- Cho, M. A., O. Malahlela, and A. Ramoelo. 2015. "Assessing the Utility WorldView-2 Imagery for Tree Species Mapping in South African Subtropical Humid Forest and the Conservation Implications: Dukuduku Forest Patch as Case Study." *International Journal of Applied Earth Observation and Geoinformation* 38: 349–357. doi:10.1016/j.jag.2015.01.015.
- Cochrane, M. A. 2000. "Using Vegetation Reflectance Variability for Species Level Classification of Hyperspectral Data." *International Journal of Remote Sensing* 21 (10): 2075–2087. doi:10.1080/01431160050021303.
- Colgan, M. S., C. A. Baldeck, J. B. Féret, and G. P. Asner. 2012. "Mapping Savanna Tree Species at Ecosystem Scales Using Support Vector Machine Classification and BRDF Correction on Airborne Hyperspectral and LiDAR Data." *Remote Sensing* 4 (11): 3462–3480. doi:10.3390/rs4113462.
- Dalponte, M., L. Bruzzone, and D. Gianelle. 2008. "Fusion of Hyperspectral and LIDAR Remote Sensing Data for Classification of Complex Forest Areas." *IEEE Transactions on Geoscience and Remote Sensing* 46 (5): 1416–1427. doi:10.1109/TGRS.2008.916480.
- Dalponte, M., H. O. Ørka, T. Gobakken, D. Gianelle, and E. Næsset. 2013. "Tree Species Classification in Boreal Forests with Hyperspectral Data." *IEEE Transactions on Geoscience and Remote Sensing* 51 (5): 2632–2645. doi:10.1109/TGRS.2012.2216272.
- Donoghue, D. N. M., P. J. Watt, N. J. Cox, and J. Wilson. 2007. "Remote Sensing of Species Mixtures in Conifer Plantations Using LiDAR Height and Intensity Data." *Remote Sensing of Environment* 110 (4): 509–522. doi:10.1016/j.rse.2007.02.032.
- Dwyer, J. F., D. J. Nowak, and M. H. Noble. 2003. "Sustaining Urban Forests." *Journal of Arboriculture* 29 (1): 49–55.

- Eamus, D., A. Huete, and Q. Yu. 2016. "Vegetation Dynamics: a Synthesis of Plant Ecophysiology." *Remote Sensing and Modelling*. New York: Cambridge University Press.
- Eitel, J. U. H., L. A. Bernhard Höfle, A. A. Vierling, A. Abellán, G. P. Asner, J. S. Deems, C. L. Glennie, et al. 2016. "Beyond 3-D: The New Spectrum of Lidar Applications for Earth and Ecological Sciences." *Remote Sensing of Environment* 186: 372–392. doi:10.1016/j.rse.2016.08.018.
- Evans, J. S., and M. A. Murphy. 2014. "Rfutilities." *R Package Version 1.0-0*. <http://CRAN.R-project.org/package=rfUtilities>
- Fang, F., J. Im, J. Lee, and K. Kim. 2016. "An Improved Tree Crown Delineation Method Based on Live Crown Ratios from Airborne LiDAR Data." *GIScience and Remote Sensing* 53 (3): 402–419. doi:10.1080/15481603.2016.1158774.
- Fassnacht, F. E., H. Latifi, K. Stereńczak, A. Modzelewska, M. Lefsky, L. T. Waser, C. Straub, and A. Ghosh. 2016. "Review of Studies on Tree Species Classification from Remotely Sensed Data." *Remote Sensing of Environment*. doi:10.1016/j.rse.2016.08.013.
- Ganguly, S., M. A. Friedl, B. Tan, X. Zhang, and M. Verma. 2010. "Land Surface Phenology from MODIS: Characterization of the Collection 5 Global Land Cover Dynamics Product." *Remote Sensing of Environment* 114 (8): 1805–1816. doi:10.1016/j.rse.2010.04.005.
- Gates, D. M., H. J. Keegan, J. C. Schleiter, and V. R. Weidner. 1965. "Spectral Properties of Plants." *Applied Optics* 4 (1): 11. doi:10.1364/AO.4.000011.
- Ghosh, A., F. E. Fassnacht, P. K. Joshi, and B. Kochb. 2014. "A Framework for Mapping Tree Species Combining Hyperspectral and LiDAR Data: Role of Selected Classifiers and Sensor across Three Spatial Scales." *International Journal of Applied Earth Observation and Geoinformation* 26 (1): 49–63. doi:10.1016/j.jag.2013.05.017.
- Haralick, R. M., K. Shanmugam, and I. H. Dinstein. 1973. "Textural Features for Image Classification." *IEEE Transactions on Systems, Man, and Cybernetics* SMC-3 (6): 610–621. doi:10.1109/TSMC.1973.4309314.
- He, Y., Y. Bo, R. de Jong, A. Li, Y. Zhu, and J. Cheng. 2015. "Comparison of Vegetation Phenological Metrics Extracted from GIMMS NDVIg and MERIS MTCI Data Sets over China." *International Journal of Remote Sensing* 36 (1): 300–317. doi:10.1080/01431161.2014.994719.
- Heinzel, J., and B. Koch. 2011. "Exploring Full-Waveform LiDAR Parameters for Tree Species Classification." *International Journal of Applied Earth Observation and Geoinformation* 13 (1): 152–160. doi:10.1016/j.jag.2010.09.010.
- Hill, R. A., A. K. Wilson, M. George, and S. A. Hinsley. 2010. "Mapping Tree Species in Temperate Deciduous Woodland Using Time-Series Multi-Spectral Data." *Applied Vegetation Science* 13 (1): 86–99. doi:10.1111/j.1654-109X.2009.01053.x.
- Holmgren, J., and Å. Persson. 2004. "Identifying Species of Individual Trees Using Airborne Laser Scanner." *Remote Sensing of Environment* 90 (4): 415–423. doi:10.1016/S0034-4257(03)00140-8.
- Hughes, G. F. 1968. "On the Mean Accuracy of Statistical Pattern Recognizers." *IEEE Transactions on Information Theory* 14 (1): 55–63. doi:10.1109/TIT.1968.1054102.
- Immitzer, M., C. Atzberger, and T. Koukal. 2012. "Tree Species Classification with Random Forest Using Very High Spatial Resolution 8-Band worldView-2 Satellite Data." *Remote Sensing* 4 (9): 2661–2693. doi:10.3390/rs4092661.
- Jones, T. G., N. C. Coops, and T. Sharma. 2010. "Assessing the Utility of Airborne Hyperspectral and LiDAR Data for Species Distribution Mapping in the Coastal Pacific Northwest, Canada." *Remote Sensing of Environment* 114 (12): 2841–2852. doi:10.1016/j.rse.2010.07.002.
- Karlson, M., M. Ostwald, H. Reese, H. R. Bazié, and B. Tankoano. 2016. "Assessing the Potential of Multi-Seasonal WorldView-2 Imagery for Mapping West African Agroforestry Tree Species." *International Journal of Applied Earth Observation and Geoinformation* 50: 80–88. doi:10.1016/j.jag.2016.03.004.
- Key, T., T. A. Warner, J. B. McGraw, and M. A. Fajvan. 2001. "A Comparison of Multispectral and Multitemporal Information in High Spatial Resolution Imagery for Classification of Individual Tree Species in A Temperate Hardwood Forest." *Remote Sensing of Environment* 75 (1): 100–112. doi:10.1016/S0034-4257(00)00159-0.
- Kim, S. 2007. "Individual tree species identification using LIDAR-derived crown structures and intensity data." Doctoral dissertation, University of Washington.

- Kim, S., R. J. McGaughey, H.-E. Andersen, and G. Schreuder. 2009. "Tree Species Differentiation Using Intensity Data Derived from Leaf-On and Leaf-Off Airborne Laser Scanner Data." *Remote Sensing of Environment* 113 (8): 1575–1586. doi:10.1016/j.rse.2009.03.017.
- Klosterman, S. T., K. Hufkens, J. M. Gray, E. Melaas, O. Sonnentag, I. Lavine, L. Mitchell, R. Norman, M. A. Friedl, and A. D. Richardson. 2014. "Evaluating Remote Sensing of Deciduous Forest Phenology at Multiple Spatial Scales Using PhenoCam Imagery." *Biogeosciences* 11 (16): 4305–4320. doi:10.5194/bg-11-4305-2014.
- Knyazikhin, Y., M. A. Schull, P. Stenberg, M. Mottus, M. Rautiainen, Y. Yang, A. Marshak, et al. 2013. "Hyperspectral Remote Sensing of Foliar Nitrogen Content." *Proceedings of the National Academy of Sciences* 110 (3): E185–E192. doi:10.1073/pnas.1210196109.
- Korpela, I., H. O. Ørka, M. Maltamo, T. Tokola, and J. Hyypä. 2010. "Tree Species Classification Using Airborne LiDAR - Effects of Stand and Tree Parameters, Downsizing of Training Set, Intensity Normalization, and Sensor Type." *Silva Fennica* 44 (2): 319–339. doi:10.14214/sf.156.
- Kuhn, M., J. Wing, S. Weston, A. Williams, C. Keefer, A. Engelhardt, T. Cooper, et al. 2016. "Caret: Classification and Regression Training." R package version 6.0-73. <https://cran.r-project.org/web/packages/caret/index.html>.
- Liu, D., and F. Xia. 2010. "Assessing Object-Based Classification: Advantages and Limitations." *Remote Sensing Letters* 1 (4): 187–194. doi:10.1080/01431161003743173.
- Liu, T., J. Im, and L. J. Quackenbush. 2015. "A Novel Transferable Individual Tree Crown Delineation Model Based on Fishing Net Dragging and Boundary Classification." *ISPRS Journal of Photogrammetry and Remote Sensing* 110: 34–47. doi:10.1016/j.isprsjprs.2015.10.002.
- Madonsela, S., M. A. Cho, R. Mathieu, O. Mutanga, A. Ramoelo, Ž. Kaszta, R. Van De Kerchove, and E. Wolff. 2017. "Multi-Phenology WorldView-2 Imagery Improves Remote Sensing of Savannah Tree Species." *International Journal of Applied Earth Observation and Geoinformation* 58: 65–73. doi:10.1016/j.jag.2017.01.018.
- Maxwell, A. E., T. A. Warner, and F. Fang. 2018. "Implementation of Machine-Learning Classification in Remote Sensing: An Applied Review." *International Journal of Remote Sensing* 39 (9): 2784–2817. doi:10.1080/01431161.2018.1433343.
- Melgani, F., and L. Bruzzone. 2004. "Classification of Hyperspectral Remote Sensing Images with Support Vector Machines." *IEEE Transactions on Geoscience and Remote Sensing* 42 (8): 1778–1790. doi:10.1109/TGRS.2004.831865.
- Mohammed, G. H., T. L. Noland, D. Irving, P. H. Sampson, P. J. Zarco-Tejada, and J. R. Miller. 2000. *Natural and Stress-Induced Effects on Leaf Spectral Reflectance in Ontario Species*. Forest Research Report No. 156. Sault Ste Marie, ON: Ontario Forest Research Institute.
- Ollinger, S. V. 2011. "Sources of Variability in Canopy Reflectance and the Convergent Properties of Plants." *New Phytologist* 189: 375–394. doi:10.1111/j.1469-8137.2010.03536.x.
- Omer, G., O. Mutanga, E. M. Abdel-Rahman, and E. Adam. 2016. "Empirical Prediction of Leaf Area Index (LAI) of Endangered Tree Species in Intact and Fragmented Indigenous Forests Ecosystems Using WorldView-2 Data and Two Robust Machine Learning Algorithms." *Remote Sensing* 8 (324): 1–26. doi:10.3390/rs8040324.
- Pu, R., and S. Landry. 2012. "A Comparative Analysis of High Spatial Resolution IKONOS and WorldView-2 Imagery for Mapping Urban Tree Species." *Remote Sensing of Environment* 124: 516–533. doi:10.1016/j.rse.2012.06.011.
- R Core Development Team. 2016. "R: A Language and Environment for Statistical Computing." Vienna, Austria: R Foundation for Statistical Computing. <https://www.R-project.org/>.
- Rautiainen, M., P. Stenberg, T. Nilson, and A. Kuusk. 2004. "The Effect of Crown Shape on the Reflectance of Coniferous Stands." *Remote Sensing of Environment* 89 (1): 41–52. doi:10.1016/j.rse.2003.10.001.
- Reed, B. C., J. F. Brown, D. VanderZee, T. R. Loveland, J. W. Merchant, and D. O. Ohlen. 1994. "Measuring Phenological Variability from Satellite Imagery." *Journal of Vegetation Science* 5 (5): 703–714. doi:10.2307/3235884.
- Reed, B. C., M. D. Schwartz, and X. Xiao. 2009. "Remote Sensing Phenology." *Phenology of Ecosystem Processes* 231–246. doi:10.1007/978-1-4419-0026-5_10.

- Sakamoto, T., M. Yokozawa, H. Toritani, M. Shibayama, N. Ishitsuka, and H. Ohno. 2005. "A Crop Phenology Detection Method Using Time-Series MODIS Data." *Remote Sensing of Environment* 96 (3–4): 366–374. doi:10.1016/j.rse.2005.03.008.
- Sayn-Wittgenstein, L. 1978. "Recognition of Tree Species on Aerial Photographs." Information report FMR-X-188. Canadian Forest Service. Dept. of the Environment. 97. Ottawa, ON: Forest Management Institute.
- Therneau, T., B. Atkinson, and B. Ripley. 2017. "Rpart: Recursive Partitioning and Regression Trees." R package version 4.1-11. <https://cran.r-project.org/web/packages/rpart/index.html>.
- Toutin, T. 2004. "Geometric Processing of Remote Sensing Images: Models, Algorithms and Methods." *International Journal of Remote Sensing* 25 (10): 1893–1924. doi:10.1080/0143116031000101611.
- Trimble. 2011. *eCognition Developer 8.64.1 User Guide*. Munich: Trimble.
- Vain, A., S. Kaasalainen, J. Hyypä, and E. Ahokas. 2009. "Calibration of Laser Scanning Intensity Data Using Brightness Targets. The Method Developed by the Finnish Geodetic Institute." *Geodesy and Cartography* 35 (3): 77–81. doi:10.3846/1392-1541.2009.35.77-81.
- Van Ewijk, K. Y., C. F. Randin, P. M. Treitz, and N. A. Scott. 2014. "Predicting Fine-Scale Tree Species Abundance Patterns Using Biotic Variables Derived from LiDAR and High Spatial Resolution Imagery." *Remote Sensing of Environment* 150: 120–131. doi:10.1016/j.rse.2014.04.026.
- Vaughn, N. R., L. M. Moskal, and E. C. Turnblom. 2012. "Tree Species Detection Accuracies Using Discrete Point Lidar and Airborne Waveform Lidar." *Remote Sensing* 4 (2): 377–403. doi:10.3390/rs4020377.
- Vauhkonen, J., H. O. Ørka, J. Holmgren, M. Dalponte, J. Heinzel, and B. Koch. 2014. "Tree Species Recognition Based on Airborne Laser Scanning and Complementary Data Sources." In *Forestry Applications of Airborne Laser Scanning*, edited by M. Maltamo, E. Naesset, and J. Vauhkonen, 1st ed., 135–156. Springer Netherlands. doi:10.1007/978-94-017-8663-8
- Verlič, A., N. Đurić, Ž. Kokalj, A. Marsetič, P. Simončič, and K. Oštir. 2014. "Tree Species Classification Using WorldView-2 Satellite Images and Laser Scanning Data in a Natural Urban Forest." *Šumarski List* 138 (9/10): str. 477–488. doi:10.3390/rs60x000x.
- Voss, M., and R. Sugumaran. 2008. "Seasonal Effect on Tree Species Classification in an Urban Environment Using Hyperspectral Data, LiDAR, and an Object-Oriented Approach." *Sensors* 8 (5): 3020–3036. doi:10.3390/s8053020.
- Warner, T. A., J. Y. Lee, J. B. McGraw, D. A. Hill, and D. G. Leckie. 1999. "Delineation and Identification of 605 Individual Trees in the Eastern Deciduous Forest." In *Proceedings of the International Forum on Automated Interpretation of High Spatial Resolution Digital Imagery for Forestry, 10–12 February, Victoria, BC, Canada*, edited by Hill, D. A and D.G. Leckie, 81–91. Victoria, Canada: Pacific Forestry Centre, Canadian Forest Service.
- Warner, T. 2011. "Kernel-Based Texture in Remote Sensing Image Classification." *Geography Compass* 5 (10): 781–798. doi:10.1111/j.1749-8198.2011.00451.x.
- Waser, L. T., M. Küchler, K. Jütte, and T. Stampfer. 2014. "Evaluating the Potential of WorldView - 2 Data to Classify Tree Species and Different Levels of Ash Mortality." *Remote Sensing* 6 (5): 4515–4545. doi:10.3390/rs6054515.
- Wolter, P. T., and P. A. Townsend. 2011. "Multi-Sensor Data Fusion for Estimating Forest Species Composition and Abundance in Northern Minnesota." *Remote Sensing of Environment* 115 (2): 671–691. doi:10.1016/j.rse.2010.10.010.
- Wolter, P. T., D. J. Mladenoff, G. E. Host, and T. R. Crow. 1995. "Improved Forest Classification in the Northern Lake States Using Multi-Temporal Landsat Imagery." *Photogrammetric Engineering and Remote Sensing* 61 (9): 1129–1143.
- Zhang, K., and B. Hu. 2012. "Individual Urban Tree Species Classification Using Very High Spatial Resolution Airborne Multi-Spectral Imagery Using Longitudinal Profiles." *Remote Sensing* 4 (6): 1741–1757. doi:10.3390/rs4061741.